Mechanistic Study of Delamination Fracture in Al-Li Alloy C458 (2099)

W. A. Tayon[1]; R. E. Crooks[2]; M. S. Domack[3]; J. A. Wagner[3];
A. J. Beaudoin[4]; R. J. McDonald[4]
[1]Old Dominion University, Norfolk, Virginia, USA ; [2]National Institute of Aerospace, Hampton, Virginia, USA; [3]NASA Langley Research Center, Hampton, Virginia, USA; [4]University of Illinois Urbana-Champaign, Urbana, Illinois, USA

Abstract:

Delamination fracture has limited the use of lightweight Al-Li alloys. In the present study, electron backscattered diffraction (EBSD) methods were used to characterize crack paths in Al-Li alloy C458 (2099). Secondary delamination cracks in fracture toughness samples showed a pronounced tendency for fracture between grain variants of the same deformation texture component. These results were analyzed by EBSD mapping methods and simulated with finite element analyses. Simulation procedures include a description of material anisotropy, local grain orientations, and fracture utilizing crystal plasticity and cohesive zone elements. Taylor factors computed for each grain orientation subjected to normal and shear stresses indicated that grain pairs with the largest Taylor factor differences were adjacent to boundaries that failed by delamination. Examination of matching delamination fracture surface pairs revealed pronounced slip bands in only one of the grains bordering the delamination. These results, along with EBSD studies, plasticity simulations, and Auger electron spectroscopy observations support a hypothesis that delamination fracture occurs due to poor slip accommodation along boundaries between grains with greatly differing plastic response.

1. Introduction

Al-Li alloys are of interest for use in aerospace structures due to the desirable combination of high strength and low density. From the earliest application in the late 1950's of alloy 2020 for aircraft structures [1] to the more recent success in the early 1990's of the application of alloy 2195 for the Space Shuttle External Tank (ET), the aerospace industry has conducted extensive research and development programs to further improve the properties of Al-Li alloys through chemistry and processing modifications [2-5]. However, Al-Li alloys with Li content greater than approximately 1.0% tend to exhibit a delamination fracture mode [6-9], which has limited their use in more widespread structural applications. Delamination fracture is characterized by failure along grain boundaries parallel to the rolling plane, which may occur in the plastic zone ahead of an advancing lateral crack [7]. Aerospace designers have found it difficult to accommodate this failure mode in design and lifetime assessments. The goal of this study was to develop a better understanding of the delamination fracture

[1] (W. Tayon) wtayo001@odu.edu

mechanisms in Al-Li alloys, which may enable processing modifications to reduce or eliminate delaminations.

Several theories have been proposed to explain the tendency for intergranular fracture in Al-Li alloys, including: planar slip [10, 11], weakening of the grain boundary due to a large area fraction of precipitates [12-15], and grain boundary segregation [16, 17]. Studies of Al-Li alloy 2090 [18] have shown that not all high angle boundaries (greater than 30° misorientation) were susceptible to delamination fracture. Recently, boundaries susceptible to delamination were found to have significant differences in Taylor factor values between the adjacent grains [19]. This difference may cause a high stress concentration; due to poor slip accommodation at the boundary, which promotes delamination fracture.

The current study investigated delamination behavior in Al-Li alloy C458 (2099) using EBSD analyses to identify grain orientations, grain boundary types and Taylor factor values. Finite element analyses and crystal plasticity theory were used to model the local grain boundary stress state associated with a global loading case. Local deformation in identified grain pairs was considered to explore the effect of large mismatch in Taylor factors across boundaries that are susceptible to delamination. Studies of delamination fracture surfaces by scanning electron microscopy (SEM) and Auger electron spectroscopy (AES) identified relevant microstructural features and localized deformation effects.

2. Material

The material evaluated in this study was Al-Li alloy C458-T8 plate, 6 cm (2 ⅜ in.) thick. The nominal composition by weight percent was 2.6 Cu, 1.7 Li, 0.6 Zn, 0.3 Mg, 0.25 Mn, 0.09 Zr, balance Al. Alloy C458, currently registered by the Aluminum Association as 2099, is similar to alloy 2090, modified to reduce strength anisotropy and improve fracture toughness [20]. The typical microstructures at the mid-plane (t/2, where t = plate thickness) and near-surface (t/8) locations of the C458 plate, shown in Fig. 1, exhibit a lamellar, pancake grain morphology, which is characteristic of Al-Li rolled products. The grains are

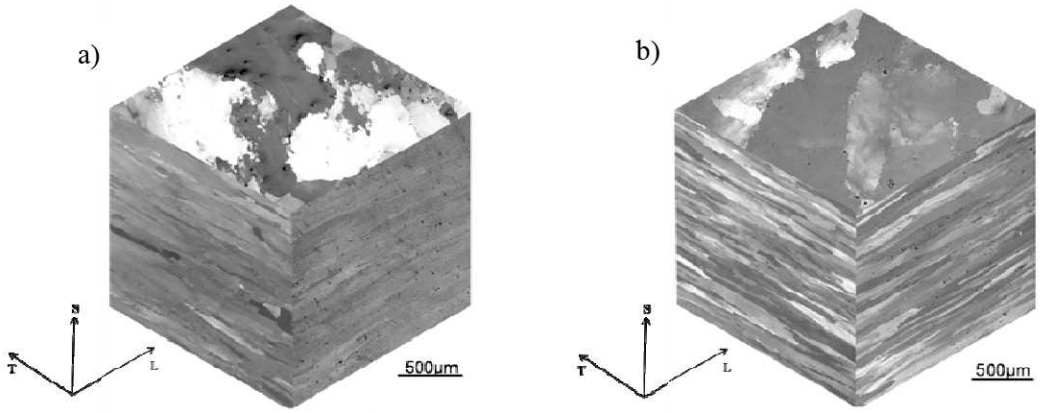

Fig. 1-Triplanar images of 6 cm thick C458 plate at two locations within the plate thickness. (a) mid-thickness (t/2) region and (b) near surface (t/8) region.

more highly elongated in the longitudinal (L), or rolling direction. Grain dimensions varied from 500 to 1,000 μm in the L direction, from 300 to 1,000 μm in the transverse direction (T) and 50 to 200 μm thick in the short transverse (S) or plate thickness direction. Differing degrees of contrast in Fig. 1 correspond to variations in grain orientation. At t/2, variations in contrast in the S direction are small, with relatively few texture components present, predominantly brass and cube as indicated by EBSD analysis. However, the microstructure at t/8 shows a wide variation of texture components (i.e. copper, cube, Goss, S, brass and several more per EBSD analysis) and a wide variation in contrast.

3. Procedure

3.1 Sample Preparation

Compact tension, C(T), fracture toughness specimens, machined from the mid-plane (t/2) of the plate in an L-T orientation were sectioned after failure. The primary crack advanced in the transverse (T) direction and delamination fractures propagated in the longitudinal (L) direction along grain boundaries parallel to the rolling direction. Samples were mechanically polished on the LS plane with a precision polishing apparatus to produce a flat and relatively strain-free surface, similar to Katrakova et al. [21], producing ESBD patterns comparable to those obtained with electropolishing [22]. Mechanical polishing was performed with an automated polishing system. The depth of material removed was monitored with a micrometer dial gauge attached to the polishing head. The polishing system allowed application of loads in increments of 100 grams over a range of 0 to 600 grams. The platen and polishing head were aligned parallel within a tolerance of 3 μm.

3.2 Electron Backscattered Diffraction (EBSD)

EBSD patterns were collected using a commercially available diffraction camera interfaced with data collection software for indexing patterns. Orientation image maps and Taylor factor maps were plotted. Orientation distribution functions (ODFs) and ODF pole figures were calculated by the harmonic series expansion method. For an accelerating voltage of 20 kV, a backscattered electron penetration depth of 50 nm or less has been estimated by Hjelen [23], and later corroborated [24]. Crisp, well-indexed patterns were obtained in the present study, indicating minimal polishing damage. A “hit rate” (percentage of indexed patterns) of 95% was routinely obtained.

3.3 Taylor Factor Computations

Taylor factors (TF) were calculated for each indexed orientation point, based on stresses believed to contribute to delamination fracture. In the present study, they were calculated from EBSD data sets using Orientation Imaging Microscopy™ (OIM™) software. A user defined strain tensor was applied from the stress components expected for the grain boundary. This employed a globally applied load case, and the slip plane and direction associated with the specific orientation.

For face-centered-cubic (fcc) materials the slip system is {111}<110>. All 12 variants of this slip system were considered in Taylor factor calculations.

For this study, a deformation gradient was chosen with a combination of normal and shear strains. Finite element simulations and mechanical test results indicated that the initiation and propagation of delamination cracks stemmed from a combination of normal and shear stresses at the grain boundary. In computational studies with copper, the development of this shear component at the boundary is attributed to elastic anisotropy between grains, accounting for the effects of crystal plasticity [25]. The assigned deformation gradient, **F**, is shown mathematically in equation (1), and is a summation of the identity and imposed strain tensors [26]. The subscripts x, y, and z used in the deformation gradient correspond the sample directions L, S, and T, respectively. Due to incompressibility of solid materials, the trace of the strain tensor must be zero; otherwise significant hydrostatic stresses would accumulate. The proposed deformation gradient is shown below to achieve reasonable Taylor factor values.

$$\mathbf{F} = \mathbf{I} + \varepsilon = \begin{bmatrix} 1+\varepsilon_{xx} & \varepsilon_{xy} & \varepsilon_{xz} \\ \varepsilon_{xy} & 1+\varepsilon_{yy} & \varepsilon_{yz} \\ \varepsilon_{xz} & \varepsilon_{yz} & 1+\varepsilon_{zz} \end{bmatrix} = \begin{bmatrix} 0.5 & 0 & 0 \\ 0 & 0.5 & 1 \\ 0 & 1 & 2 \end{bmatrix} \qquad (1)$$

3.4 Fractography

Several delaminations were sectioned to expose the matching fracture surface pairs and then examined in a scanning electron microscope (SEM). A precision saw cut was made at the tip of each delamination, allowing the matching pairs to be exposed. The matching pairs were inserted in the SEM side-by-side to examine the delamination fracture surfaces. Standard fractographic images were taken at varying magnifications and tilt angles to investigate fracture features such as slip bands and grain boundary precipitates. EBSD patterns were obtained from delamination fracture surfaces and used to correlate these features with grain orientation and boundary plane. Images of the fractured surfaces and local crystal orientation have been compared with Auger electron spectroscopy (AES) to evaluate fracture morphology, grain-to-grain deformation, and slip accommodation along delaminations.

3.5 Auger Electron Spectroscopy (AES)

Auger electron spectroscopy [27] was employed to investigate chemical species on the fracture surfaces of delaminations. Previous investigations have explored the chemistry of fracture surfaces for a variety of alloys and failure modes, including failure along grain boundaries [28]. The Auger microprobe utilizes a LaB_6 filament electron gun for excitation and a single pass cylindrical mirror analyzing detector. AES relates specific electron energy peaks with chemical composition. Detection of Li is difficult in Al-Cu-Li-X alloys due to interference between Li and Al peaks, however variations in copper content are relatively easy to detect. Variations in copper concentrations on the fracture surfaces were used

to identify locations of Cu-rich precipitates (possibly the T_1, Al_2LiCu, phase) on the delamination surfaces.

3.6 Plasticity Simulations

A crystal plasticity model was developed, based on measured material properties from experimental studies of Al-Li alloys. Briefly, a finite element mesh developed for small scale yielding in plane strain was complemented with cohesive zone elements in the primary crack and delamination regions. An analytical plane strain K_I field displacement with a "far-field" maximum value K_I = 47 MPa$\sqrt{m}$ was imposed. Cohesive zone properties for the primary crack realized a $K_{Ic} \approx 31$ MPa$\sqrt{m}$. The ratio of primary crack strength to yield strength was taken to be 3, typical of 2XXX alloys. A 2:1 ratio in strength between the primary crack and the delamination was prescribed. Further, it was necessary to increase the primary crack energy relative to the delamination energy by a factor of 5 to develop a realistic delamination geometry, and have the delamination "run ahead" of the primary crack.

4. EBSD Results

4.1 Texture and Grain Orientation

In a rolled, unrecrystallized, aluminum plate, a strong deformation texture may develop with peak intensities near the ideal brass, copper and S texture orientations. The "brass" orientation is often strong in Zr containing alloys such as Al-Li-Zr, Al-Cu-Zr, and Al-Cu-Li alloys [7, 18, 29-31]. At the mid-thickness of rolled Al-Li alloy plate (t/2), the texture is typically dominated by the brass orientation, and C458 is no exception. Brass (Bs) has two variants, equivalent to a 180° rotation about the non-symmetric rolling direction axis, $<2\bar{1}1>$. In this study, we designate Bs1 by the Euler angles (35, 45, 0) or Miller indices $(011)[2\bar{1}1]$ and Bs2 by the Euler angles (55, 90, 45) or the Miller indices $(011)[1\bar{1}2]$.

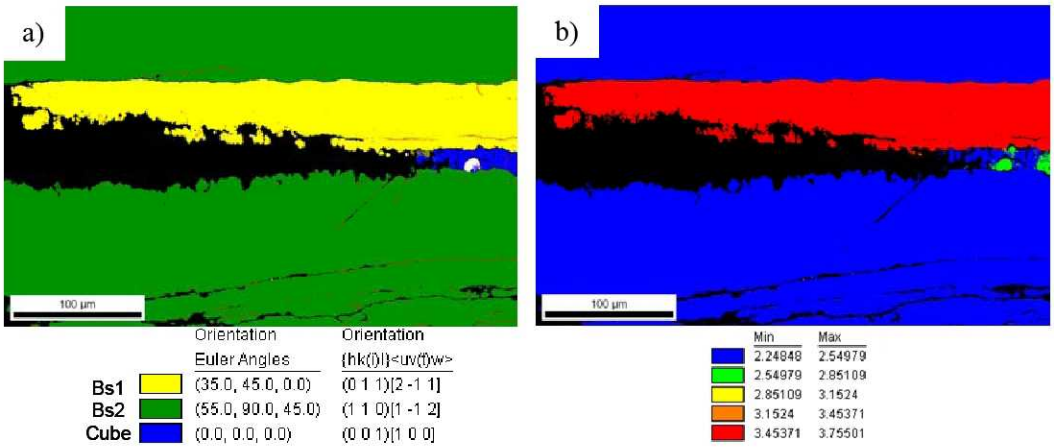

Fig. 2- Comparison of (a) local grain orientation and (b) Taylor factor values around a typical delamination.

Delamination cracks in Al-Li alloys tend to occur along high angle grain boundaries with misorientations greater than 30º [18]. In this study of fracture toughness specimens, all delaminations occurred along grain boundaries with misorientations between 50º and 60º. In alloy C458, a tendency for intergranular fracture between brass texture variants was observed in the delaminations studied as shown in Fig. 2a. While most delaminations occurred between brass variants, delamination did also occur between brass and cube grains.

4.2 Taylor Factor Analysis

Taylor factor (TF) values were calculated and plotted for grain orientations within EBSD scans of delaminations. As stated, delaminations frequently occurred along boundaries between brass variants. The largest differences in TF across boundaries corresponded with the location of delaminations. Typically, one brass variant had a lower TF value, e.g. 2.4, while the brass variant on the opposing side had a value near 3.5. These results (Fig. 2b) show a correlation between delamination fracture and TF values; delaminations occur along boundaries between grains with a distinct orientation difference – one which results in the largest TF difference. Such TF differences arise fundamentally due to the relationship of the specific grain orientation relative to the applied stress conditions during testing. When high and low TF grains share a common boundary, these locations display an increased vulnerability to fracture. Through the application of Taylor factors computed as a function of grain orientation and loading environment, it is possible to identify vulnerable locations within the microstructure and predict the location of potential delamination fractures.

5. Fractography Studies

5.1 Development of Preferential Slip Bands

Matching pairs of delamination fracture surfaces examined in an SEM revealed varying degrees of slip band formation, as shown in Fig. 3. A separated subgrain

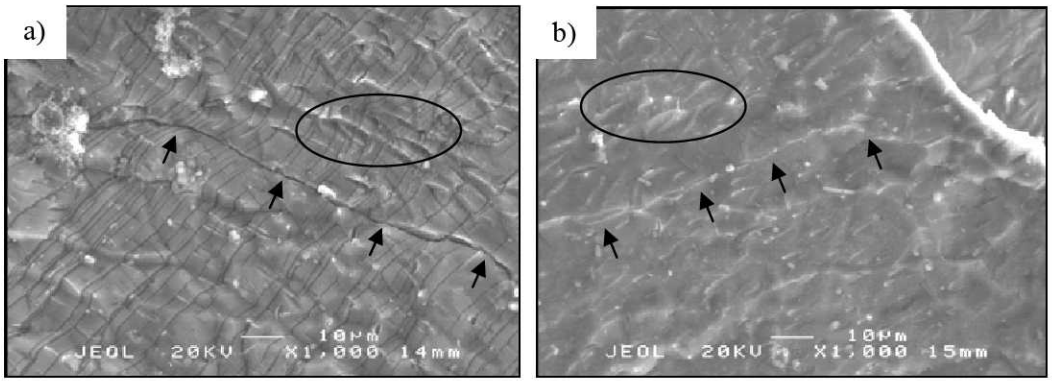

Fig. 3- SEM images of delamination fracture surface. (a) Cube grain with slip bands and (b) brass grain on opposing side. Arrows indicate a separated sub-grain boundary; encircled regions denote (b) raised ridges and (a) associated recessed pull-out features.

boundary is noted by arrows to illustrate the mirror image alignment of the fractographs. EBSD patterns were obtained along the fracture surface to

determine the grain orientations. Intense slip bands were found to systematically occur in only one grain of the observed grain pairs. Fig. 3 illustrates this finding in a cube/brass grain pair where slip bands were observed in the cube oriented grain (Fig. 3a), while no slip bands were found in the brass oriented grain (Fig. 3b). In this case, the cube grain appears to be favorably aligned for slip, possibly easy glide, while the brass grain did not exhibit deformation. Similar observations were noted where delaminations occurred between brass/brass grain pairs, with slip bands observed in only one of the two brass variants.

5.2 T_1 Precipitate Plate Separation

Further examination of the delamination fracture surfaces of the matching pairs revealed wedge-shaped features, encircled in Fig. 3, appearing as raised ridges on one surface (Fig. 3b) and recessed wedges on the other surface (Fig. 3a). One part of the wedge-shaped feature was flat and rather smooth, while the other side had a wavy appearance. These wedge-shaped features were generally 6-10μm in length, ~0.5μm in width, and less than 0.2μm in depth. Results from Auger analysis of a similarly featured region is shown in Fig. 4, where numbered features in Fig. 4a correspond with the Cu concentrations, as indicated in Fig. 4b. Raised ridge-like features were found in general to be associated with high Cu concentrations in comparison to the surrounding area. These ridges may be related to Cu-containing T_1 precipitate plates that have separated from the recessed wedge-shaped features. Furthermore, the Auger results show a concentration of precipitates on some grains but not others. These precipitate plates grow on grain boundaries with one surface coherent with the grain providing the {111} habit plane and the other surface incoherent. It is likely that the precipitates adhere to the grain providing the habit plane.

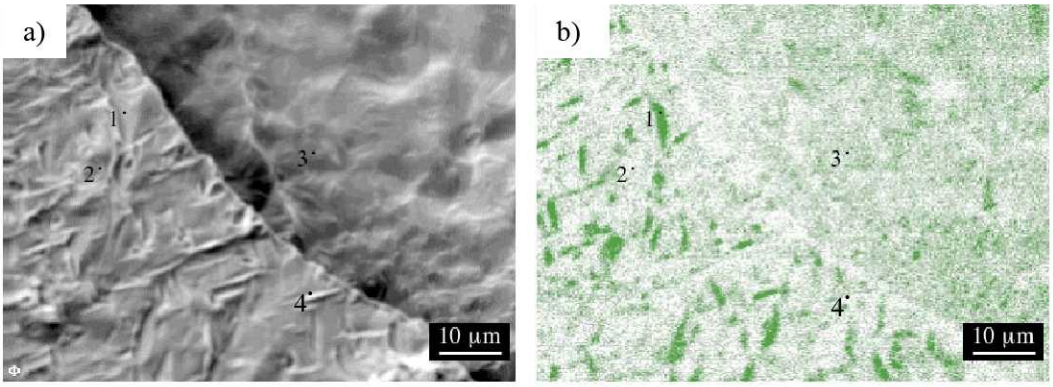

Fig. 4- (a) SEM image of mapped region and (b) the corresponding Cu concentrations from Auger electron spectroscopy.

6. Simulation Results

In finite element simulations of delamination fracture, orientations of the two brass variants (Bs1 and Bs2) were specified on opposing sides of the delamination plane, as indicated by EBSD results. A plot of the internal variable indicating failure of the cohesive zone element is shown in Fig. 5a, where failure is indicated

by a value of 1. The upper and lower plots are of the delamination and primary crack planes, respectively. The delamination proceeds ahead of the primary crack, as observed in experiment. There is a clear asymmetry of the crack growth in the primary crack plane, indicating prevalence for increased deformation in one grain. Also notable is a retarding of primary crack growth proximal to the delamination plane. Failure on the delamination plane renders a loss of constraint and promotes a localized state of plane stress. This is reflected in the micrograph of Fig. 5b, showing an image of the LS plane. It appears that "shear lips" (at arrows) are developing in response to the relief of stress along the delamination plane.

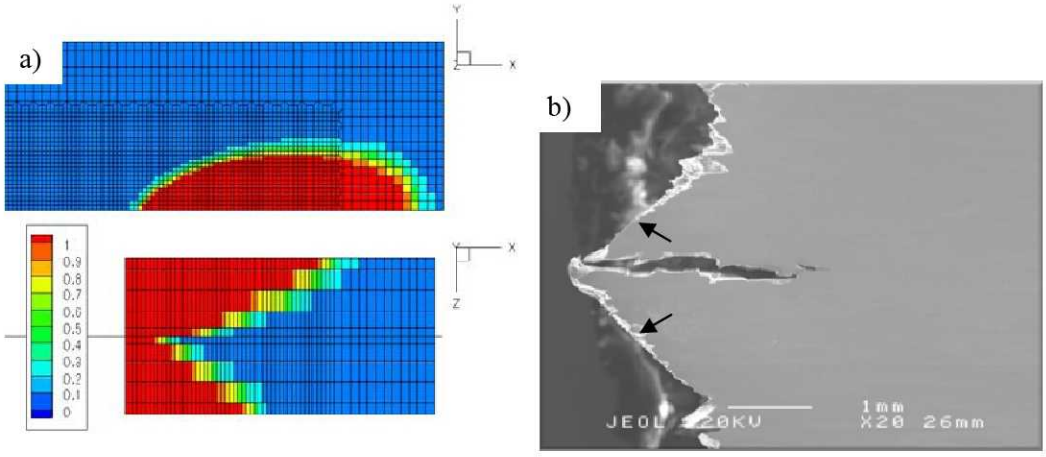

Fig. 5- (a) Crystal plasticity simulation results for a delamination between Bs1/Bs2 grains. Results are plotted for the delamination crack (top) and the primary crack (bottom). (b) Micrograph illustrating formation of "shear lips" at the site of delamination, representative of a local plane stress condition.

7. Conclusions

Previous studies in Al-Li alloys have failed to develop a conclusive explanation for the mechanisms that control delamination fracture. However, results from the current study of C458 suggest that delamination fracture occurs due to a lack of slip accommodation along boundaries between grains of greatly differing plastic response. Several critical observations were made in the current study by various experimental methods to support this hypothesis:

- Delaminations were typically found to occur between variants of the brass texture component.
- The largest differences in Taylor factors occurred when brass variants were paired within the microstructure.
- Studies of the paired fracture surfaces of delaminations revealed preferential slip band formation on one side of the fracture.
- Plasticity simulations indicated anisotropic deformation along boundaries bordered by brass texture variants.

Additionally, the observation of Cu rich areas occurring preferentially in only one grain bordering a delamination pair suggests that the T_1 precipitate may have a role in the delamination fracture process and is now under investigation.

Acknowledgement

This research was supported by the National Institute of Aerospace (NIA) and NASA Langley Research Center (Activity number 2603). The AES work was supported by the U.S. Department of Energy, Division of Materials Sciences under Award No. DEFG02-91ER45439, through the help of N. Finnegan and P. Kurath in the Frederick Seitz Materials Research Laboratory at the University of Illinois, Urbana-Champaign.

References

[1] T. Pasang, S.P. Lynch, S. Moutsos, Challenges in developing high performance Al-Li alloys. Int J Soc Mater Eng Resour 14 (2006) 7-11.
[2] C. Giummarra, B. Thomas, R. Rioja, Fabrication methods to manufacture isotropic Al-Li alloys and products for space and aerospace applications, Light Metals Technology Conference, Quebec, 2007, pp. 1-6.
[3] R.J. Rioja, Fabrication methods to manufacture isotropic Al-Li alloys and products for space and aerospace applications. Mater Sci and Eng: A 257 (1998) 100-107.
[4] A. Cho, W. Lisagor, T. Bales, Development and processing improvement of aerospace aluminum litjium alloys. NASA Technical Report Server NASA/CR-2007-215093 (2007) 1-227.
[5] B.M. Gable, A.W. Zhu, A.A. Csontos, E.A. Starke, The role of plastic deformation on the competitive microstructural evolution and mechanical properties of a novel Al-Li-Cu-X alloy. J Light Metals 1 (2001) 1-14.
[6] H. Babel, J. Gibson, M. Tarkanian, C. Parrish, M. Prietto, A. Ordonez-Chu, H. Haberl, J. Kabisch, R. Clark, J. Ogren, O.S. Es Said, 2099 Aluminum-Lithium with key-locked inserts for aerospace applications. J Mater Eng and Performance 16 (2007) 584-591.
[7] J. Wagner, R. Gangloff, Fracture toughness of an Al-Li-Cu-In alloy. Scr Metall 26 (1992) 1779-1784.
[8] J. Glazer, S. Verzasconi, R. Sawtell, Mechanical Behavior of Aluminum-Lithium Alloys at Cryogenic Temperatures. Metall and Mater Trans A 18A (1987) 1695-1701.
[9] K.V. Rao, W. Yu, R. Ritchie, Cryogenic Toughness of Commercial Aluminum-Lithium Alloys: Role of Delamination Toughening. Metall and Mater Trans A 20A (1989) 485-497.
[10] T.H. Sanders, E.A. Starke, The effect of slip distribution on the monotonic and cyclic ductility of Al---Li binary alloys. Acta Metall 30 (1982) 927-939.
[11] A.A. Csontos, E.A. Starke, The effect of inhomogeneous plastic deformation on the ductility and fracture behavior of age hardenable aluminum alloys. Int J Plast 21 (2005) 1097-1118.
[12] K.V. Jata, A.K. Vasudevan, Effect of fabrication and microstructure on the fracture initiation and growth toughness of Al-Li-Cu alloys. Mater Sci and Eng A241 (1998) 104-113.
[13] S. Suresh, A.K. Vasudevan, M. Tosten, P.R. Howell, Microscopic and macroscopic aspects of fracture in lithium-containing aluminum alloys. Acta Metall 35 (1987) 25-46.
[14] A.K. Vasudévan, R.D. Doherty, Grain boundary ductile fracture in precipitation hardened aluminum alloys. Acta Metall 35 (1987) 1193-1219.
[15] A.K. Vasudévan, E.A. Ludwiczak, S.F. Baumann, R.D. Doherty, M.M. Kersker, Fracture behavior in Al---Li alloys: role of grain boundary [delta]. Mater Sci and Eng A72 (1985) 25-30.

[16] S.P. Lynch, Fracture of 8090 Al---Li plate I. Short transverse fracture toughness. Mater Sci and Eng A136 (1991) 25-43.
[17] S.P. Lynch, B.C. Muddle, T. Pasang, Ductile-to-brittle fracture transitions in 8090 Al-Li alloys. Acta Mater 49 (2001) 2863-2874.
[18] R. Crooks, M. Domack, J. Wagner, Microtexture and nanoindentation study of delamination cracking in Al-Cu-Li-X alloys, High Performance Structures and Materials III, Brussels, Belgium, 2006, pp. 549-558.
[19] W. Tayon, R. Crooks, M. Domack, J. Wagner, A.A. Elmustafa, ESBD study of delamination fracture in Al-Li alloy 2090. J Exp Mech (In Press).
[20] M. Romios, R. Tiraschi, J. Ogren, O. Es-Said, C. Parrish, H. Babel, Design of multistep aging treatments of 2099 (C458) Al-Li alloy. J Mater Eng and Performance 14 (2005) 641-646.
[21] D. Katrakova, F. Mucklich, Specimen preparation and electron backscatter diffraction- Part I: metals. Practical Metall 38 (2001) 547-565.
[22] G.L. Wynick, C.J. Boehlert, Use of electropolishing for enhanced metallic specimen preparation for electron backscatter diffraction analysis. Mater Charact 55 (2005) 190-202.
[23] J. Hjelen, E. Nes, in XIIth Int. Cong on Electron Microscopy, Seattle, 1990.
[24] K.Z. Baba-Kishi, Review Electron backscatter Kikuchi diffraction in the scanning electron microscope for crystallographic analysis. J Mater Sci 37 (2002) 1715-1746.
[25] H.H. Fu, D.J. Benson, M. André Meyers, Computational description of nanocrystalline deformation based on crystal plasticity. Acta Mater 52 (2004) 4413-4425.
[26] U.F. Kocks, C. Tome, H. Wenk, Texture and anisotropy: preferred orientations in polycrystals and their effect on materials properties, Cambridge University Press, Cambridge, 1998.
[27] J.T. Grant, Surface analyis with Auger electron spectroscopy. Applications of Surface Science 13 (1982) 35-62.
[28] D.F. Stein, Applications of Auger spectroscopy to materials research. J. Vac. Sci. Technol. 12.1 (1975) 268-275.
[29] T. McNelley, D. Swisher, M. Pérez-Prado, Deformation bands and the formation of grain boundaries in a superplastic aluminum alloy. Metall and Mater Trans A 33 (2002) 279-290.
[30] P.S. Bate, Y. Huang, F.J. Humphreys, Development of the "brass" texture component during the hot deformation of Al-6Cu-0.4Zr. Acta Mater 52 (2004) 4281-4289.
[31] R. Crooks, Z. Wang, V. Levit, R. Shenoy, Microtexture, microstructure and plastic anisotropy of AA2195. Mater Sci and Eng A257 (1998) 145-152.